Link Budget Assessment for GEO Feeder Links based on Optical Technology*

Ricardo Barrios[1]†, Svilen Dimitrov[2], Ramon Mata-Calvo[2], Dirk Giggenbach[2]

[1] Central Research and Technology (XRC), Airbus Group, Taufkirchen, Germany
[2] Satellite Networks Department, German Aerospace Center (DLR), 82234 Wessling, Germany

Abstract

Nowadays, large geostationary orbit (GEO) satellites can offer capacities up to 260 Gbps. In the mid-term, in order to cope with the forecasted traffic demand, multibeam high throughput satellite systems are already being deployed. Optical GEO feeder link technology may provide transmission data rates up to the order of several Terabits per second by making use of wavelength division multiplexing schemes. This work identifies physical layer techniques that enable the transmission of DVB-S2X RF modulated signals over optical carriers. The techniques reported here are the analog transparent (AT), digital transparent (DT), and the digital regenerative schemes, which require different satellite payload architectures. The effects of atmospheric turbulence over the traveling wave are addressed and discussed, along with a methodology to calculate the link budget in the feeder uplink channel. Link budget calculations for two different selected ground station locations are presented, for the both the AT and DT options. It is shown that for high altitude locations the transmission using the AT and DT options works well. For mid-altitude locations, typical 36 MHz signal are feasible, while for higher bandwidths the DT option could work when an error correction code is used.

Keywords: *Tbit/s satellite; optical feeder link; radio over FSO; scintillation; turbulent optical channel*

1 Introduction

The current telecommunications marketplace is experiencing an ever increasing demand for high-speed services, and the traffic demand for satellite broadband is expected to grow six-fold by 2020 [1]. Nowadays, large geostationary orbit (GEO) satellites can offer capacities up to 260 Gbps [2, 3, 4]. The digital agenda of the European Commission aims to provide to all European households Internet rates above 30 Mbps, with at least 50 % of the users accessing 100 Mbps or more [5]. To meet this goal satcom providers need to aim for Terabit/s capacity satellites. In the mid-term, in order to cope with the forecasted traffic, multibeam high throughput satellite (HTS) systems are already being deployed. The available radiofrequency (RF) bands to support the feeder link are in shortage to support such capacity, and a relative high number of RF gateways (GW) stations are needed to serve future HTS, e.g. in the order of 50 [1], significantly influencing the deployment cost of the overall system.

Under this scenario, optical GEO feeder link (OGEOFL) technology may provide transmission data rates up to the order of several Terabits per second by making use of wavelength division multiplexing (WDM) schemes, to support HTS systems in the midterm future. The high available bandwidth for an optical carrier reduces the number of required optical ground stations (OGS) to a single OGS station [6], in order to cope with the overall throughput required by the HTS. Although, OGS's are prone to cloud blockage and location diversity is needed to achieve carrier-class availability, the deployment of an OGS network only consists of about ten OGS's [7, 8, 9].

The aim of this paper is to identify physical layer techniques that enable the transmitting RF modulated signals—based on the DVB-S2X standard [10, 11, 12]—encapsulated over optical wavelengths along with the necessary optical technology relevant to GEO feeder links. These techniques are commonly known as Radio over Free-Space Optics (RoFSO) communications. Although successful Terabit/s data rate transmission from ground to a GEO satellite has not been reported yet, recently there has been many efforts paving the way for that goal. During the project THRUST, the German Aerospace Center (DLR) demonstrated the feasibility of the dense wavelength division multiplexing (DWDM) technology over a worst-case atmospheric channel, and have have set world-records with a 1,72 Tbps transmission in 2016, [13] and 13,16 Tbps in 2017 using commercial fibre-based communication systems [14].

The remainder of this document is organized as follows. In Section 2, the different aspects in modeling the OGEOFL uplink channel are presented. Next, in Section 3, the different techniques to implement an OGEOFL identified are explained, where basics on how RF signals can be transported with optical carriers are addressed. Section 4 is devoted

*This is the accepted version of the following article: *Barrios R, Dimitrov S, Mata-Calvo R, Giggenbach D. Link budget assessment for GEO feeder links based on optical technology. Int J Satell Commun Network. 2020; 1-18*, which has been published in final form at https://doi.org/10.1002/sat.1371. This article may be used for non-commercial purposes in accordance with the Wiley Self-Archiving Policy [http://www.wileyauthors.com/self-archiving].

†Corresponding author: ricardo.barrios@airbus.com

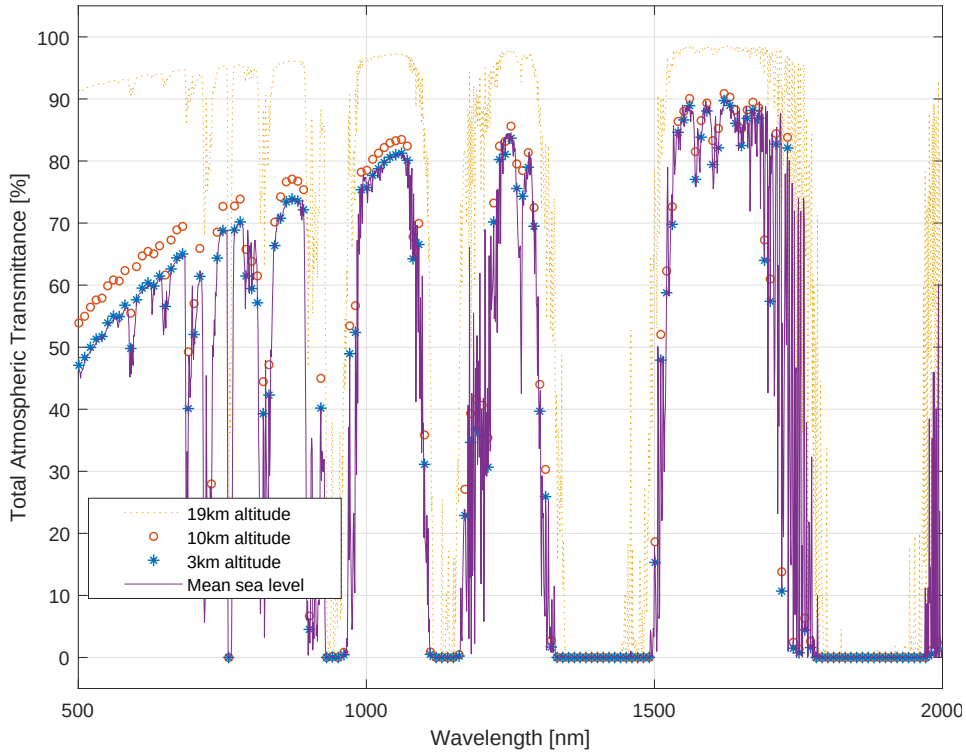

Figure 1: (Color online) Atmospheric transmittance for different wavelengths in the zenith direction, for three different altitudes.

to address the different aspects that play role in the calculation of a link budget for OGEOFL. Although this work is mainly focused on the uplink channel, i.e. the forward link of HTS systems, the specifics on how to calculate the link budget in the downlink are also presented. Additionally, Section 4 presents the link budget, using the analog transparent (AT) and digital transport (DT) options, for two different European locations. Finally, Section 5 elaborates on the conclusions drawn in this work.

2 Atmospheric optical channel model

This section elaborates on the relevant parameters involved in the optical channel definition under the turbulent atmosphere. All the different factors described below ultimately define the overall performance of a GEO feeder link that makes use of optical carriers for data transmission between an Earth based gateway and a GEO satellite.

2.1 Wavelength Selection

A laser beam traveling through the turbulent atmosphere is affected by extinction due to aerosols and molecules suspended in the air. The transmittance of the atmosphere can be expressed by Beer's law as [15]

$$L_{\mathrm{ATM}}(L) = \frac{P(L)}{P(0)} = \exp\left(-\int_0^L \alpha_{\mathrm{a}}(z,\lambda)dz\right) \tag{1}$$

where $P(0)$ is the transmitted laser power at the source, and $P(L)$ is the laser power at a distance L.

The total extinction coefficient $\alpha_{\mathrm{a}}(z,\lambda)$, which represents the extinction level along the propagation path, comprises four different phenomena, namely, molecular and aerosol scattering, and molecular and aerosol absorption. The molecular and aerosol behavior for the scattering and absorption process is wavelength dependent, thus some atmospheric windows appear where the transmission of certain optical wavelengths is more favored.

The spectral transmittance of the atmosphere presented in Figure 1, clearly exhibiting the existence of various atmospheric windows in the visible and near infrared region. Free-space optical (FSO) communications use the 850, 1300 and 1550 nm windows, and there are standard components available, as sources and detectors, which have been developed for fiber systems that can be readily used in FSO scenarios. Regarding the space qualification and usability, the 850 nm components possess the advantage in this regard as many demonstrations have been performed already, such as the inter-satellite SILEX experiment [16], the LOLA laser link [17], and also ground to GEO experiment [18]. Also, communication systems for inter-satellite links using the 1064 nm wavelength has been demonstrated in space, using the BPSK coherent laser communication terminal (LCT) built by the German company TESAT [19, 20].

The 1550 nm window is the most promising for its application in optical GEO feeder links, as a vast amount of components allow for the implementation of DWDM schemes, which will enable to reach the Tbit/s threshold in future

generations of HTS for communication. Additionally, atmospheric turbulence degradation is wavelength dependent and the larger the wavelengths the smaller the distorting effects. Nevertheless, space qualification for components in the 1550 nm transmission window is the less mature, although it is expected that most of the components necessary for implementing DWM systems are space qualified in the next 10 years. In general, WDM is an optical technology that allow for transmission of multiple wavelengths through the same channel, be it fiber or free-space, thus increasing the aggregate bandwidth available at the expense of additional power consumption [21]. On the one hand, coarse WDM systems are those that can transport up to 18 wavelengths, with channel separation of 20 nm, allowing for relaxed laser wavelength stability tolerances and wide pass-band filter. On the other hand, DWDM systems are characterized by the narrow channel spacing, where possible bandwidths are 12.5, 25, 50 and 100 GHz—which correspond to 0.1, 0.2, 0.4 and 0.8 nm, respectively—according to the ITU recommendation G.694.1 [22]. All available channels are enclosed between 1530 and 1565 nm, which comprise the optical C band, and wavelengths between 1565 and 1625 nm, which correspond to the optical L band. The small channel separation in DWDM systems requires maximum laser wavelength stability to avoid cross-talk; and special attention to the total optical power to be coupled in a fiber—due to the large number of channel—in terms of damage and nonlinear effects.

It is noteworthy to mention that up to date there has been a series of demonstrations of ground-space optical links [23, 24, 25, 26], based on 1550 nm systems, using the Lunar Lasercom Space Terminal (LLST) onboard the NASA's Lunar Atmospheric Dust and Environment Explorer (LADEE) with maximum up- and downlink rates of 20 and 622 Mbps, respectively [27]. The Optical Payload for Lasercomm Science (OPALS) system—also developed by NASA—is a low-cost terminal using OOK and Reed-Solomon forward FEC recently demonstrated an optical downlink of a pre-encoded video file at 50 Mbps on a 1550 nm optical carrier [28].

2.2 Atmospheric Turbulence

The atmospheric turbulence can be characterized by the strength of the refractive index fluctuations represented by the refractive index structure parameter C_n^2 in units of $\mathrm{m}^{-2/3}$. When a vertical path is considered, as in a feeder link scenario, the behavior of C_n^2 is mainly affected by temperature changes along the different layers within the Earth's atmosphere. Therefore, the refractive index structure parameter becomes a function of the height h above the ground level. The most widespread C_n^2 profile model is the Hufnagel-Valley (HV), best suited for inland daytime and nighttime conditions. A modified version of the HV model including the ground layer atmospheric effects on an OGS not located at sea level, and it is expressed by [29]

$$C_n^2(h) = Ae^{-\mathrm{H_{OGS}}/700}e^{-(h-\mathrm{H_{OGS}})/100} + 5.94\times10^{-53}\left(\frac{v}{27}\right)^2 h^{10}e^{-h/1000} + 2.7\times10^{-16}e^{-h/1500}, \tag{2}$$

where $A = 1.7\times10^{-14}\ \mathrm{m}^{-2/3}$ is the typical value refractive index structure parameter at ground level as recommended by the ITU [30], $v = 21\ \mathrm{m\,s}^{-1}$ is the root-mean-squared (RMS) wind speed, which are the standard values for the HV C_n^2 model for daytime conditions, and $\mathrm{H_{OGS}}$ is the optical ground station altitude above the mean sea level.

2.3 Isoplanatic Angle and Point-Ahead Angle

The geometric situation in an optical link to a geostationary satellite, presented in Figure 2, is defined mainly by three angles, namely the uplink beam divergence θ_B, the point-ahead angle θ_PAA—typically 18 μrad for a geostationary satellite—due to the relative velocity of the satellite versus the optical ground station, and the isoplanatic angle (IPA) θ_0 of the atmospheric index-of-refraction turbulence (IRT) structure, which is defined by Eq. (30) in [31, Ch. 12].

The uplink beam divergence should be made as small as possible to produce the highest signal intensity at the satellite. However, the IRT-induced beam spread sets a lower limit to this angle. When pointing the laser beam towards the satellite, the atmospheric beam-wander should be compensated by tracking the angle-of-arrival (AoA, caused by IRT) of a reference signal from the satellite, and pointing the outgoing beam accordingly. However, here the IPA sets a limit, as incoming and outgoing beams travels through different atmospheric volumes when $\theta_0 < \theta_\mathrm{PAA}$. While the magnitude of the IPA depends on the local IRT-profile structure and the wavelength, this condition is usually the case for low link elevations, as here the IPA becomes very small. This leads to a situation in which the observed AoA can no longer serve as reference for pointing the uplink beam in the correct direction to compensate atmospheric beam-wander deviations—i.e. beam tracking for the uplink is not possible. Under such conditions, increasing the uplink beam divergence, and consequently reduced received power due to the larger spot size, will decrease the influence of beam wandering relative to the size of the beam at the satellite receiver plane. This scenario imposes a challenging link budget in any low-elevation satellite-uplink, i.e. elevation angles below 30-40° depending on channel parameters, requiring very high transmit powers from ground. The effect of misspointing and some turbulence mitigation techniques has been analyzed and verified in a OGS-GEO measurement campaign [18].

2.4 IRT-related Parameters

The Fried's parameter r_0 measures the integrated turbulence strength along the optical path through the atmosphere, where smaller r_0 values correspond to stronger atmospheric index-of-refraction turbulence conditions. The Fried

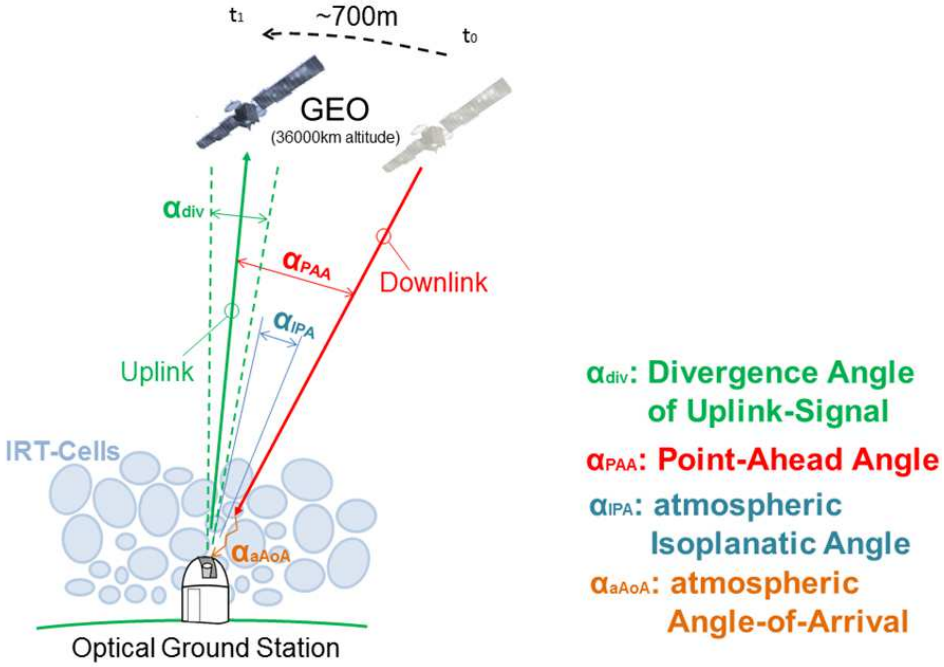

Figure 2: Scenario for an optical GEO feeder link. The satellite moves approximately 700 m during the time of flight of down- and uplink, resulting in a PAA of 18 μrad.

parameter is given by [32]

$$r_0 = \left[0.42 \sec(\zeta) k^2 \int_{\mathrm{H_{OGS}}}^{H} C_n^2(h) dh\right]^{-3/5}. \tag{3}$$

On the other hand, beam wander $\langle r_c^2 \rangle$ measures the average displacement of the beam at the receiver from the boresight, while the angular beam wander gives the same information but referred as an angular tilt at the transmitter side. It is well known that this phenomenon is caused by the large-scale inhomogeneities due to their refractive effects. A Gaussian beam wave after propagating through the turbulent atmosphere is corrupted in such a way that the instantaneous field, at the receiver plane, greatly differs from a Gaussian shape, with the added characteristic that the beam center can exhibit major deviations from the optical axis of the link. The beam wander can be calculated as [31]

$$\langle r_c^2 \rangle = 0.5(H - H_{\mathrm{GS}})^2 \sec(\zeta) \left(\frac{\lambda}{2W_0}\right)^2 \left(\frac{2W_0}{r_0}\right)^{5/3}, \tag{4}$$

where W_0 is the beam radius at the transmitter plane. Sometimes it is useful to defined the angular beam wander $\theta_{\mathrm{BW}} = \sqrt{\langle r_c^2 \rangle}/L$, referred to the transmitter plane, to allow for easy comparison with all other angular parameters defining the optical channel.

Another effect to take into account in the propagation of an optical wavefront in the turbulent atmosphere is an extra spreading of the beam, i.e. the broadening of the beam size beyond of that expected due to pure diffraction, for the case of a laser beam. The long-term spot size for uplink channel, in a ground-to-GEO scenario, will suffer an additional decrease of the received optical power, from an extra spread given in terms of the Strehl ratio as [31]

$$\mathrm{SR} = \left[1 + \left(\frac{D_{\mathrm{T}}}{r_0}\right)^{5/3}\right]^{-6/5}, \tag{5}$$

where D_{T} is the transmitter aperture diameter at the optical ground station.

In general, the IRT can be regarded as a low-pass process characterized by a cut-off frequency known as the Greenwood frequency, defined as [33]

$$\begin{aligned} f_{\mathrm{G}} =& 2.31 \lambda^{-6/5} \left[\int_0^L C_n^2(z) V^{5/3}(z) dz\right]^{3/5}, \\ V(h) =& \omega_{\mathrm{s}} h + V_{\mathrm{g}} + 30 \exp\left[-\left(\frac{h - 9400}{4800}\right)^2\right], \end{aligned} \tag{6}$$

where $V(z)$ is the wind velocity profile along the propagation path $z = \sec(\zeta)(h - H_{\mathrm{GS}})$, $\omega_{\mathrm{s}} = 7.3 \times 10^{-5}$ rad s^{-1} is the GEO satellite slew rate, and $V_{\mathrm{g}} = 8$ m s^{-1} is the wind speed at ground level.

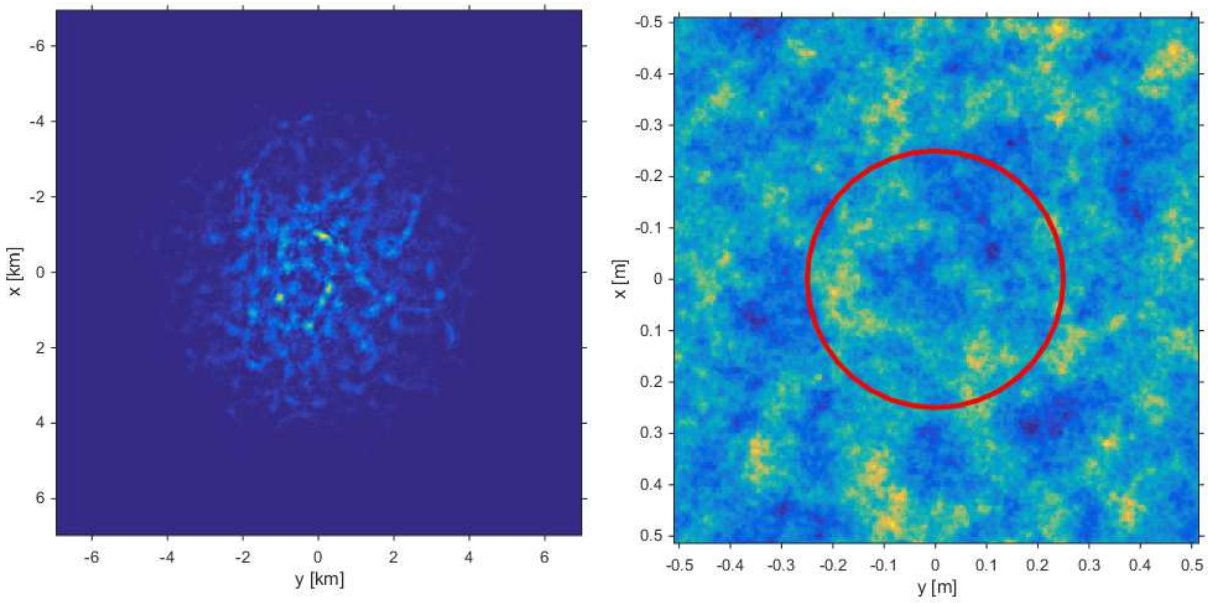

Figure 3: (Color online) Received sample fields after propagation in (left) ground-to-GEO and (right) GEO-to-ground directions. In the uplink case the speckle structure size is about 200 m, and the typical receiver size at GEO satellite is much smaller. In the downlink the speckles can be averaged by the relatively larger size of the ground receiver aperture diameter. Here a 50 cm aperture is shown.

2.5 Scintillation Index

A laser beam propagating through the atmosphere will be altered by refractive-index inhomogeneities. At the receiver plane, a random pattern is produced both in time and space [34]. The irradiance fluctuations over the receiver plane resemble the speckle phenomenon observed when a laser beam impinges over a rugged surface. The parameter that expresses these irradiance fluctuations is the scintillation index (SI), which is essentially the variance of the irradiance of the optical wave observed after propagating a distance L normalize by its mean value.

Studies on optical wave propagation traditionally are classified in two major categories, either the weak or strong fluctuations theory. It is customary to discriminate both cases for a given propagation problem by determining the value of the Rytov variance σ_R^2. The weak fluctuations regime occurs when $\sigma_R^2 < 1$, the strong fluctuations regime is associated with $\sigma_R^2 > 1$, whereas if $\sigma_R^2 \to \infty$ results in the saturation regime. The Rytov variance for a slant path can be calculated with Eq. (38) in [31, Ch. 12].

Figure 3 presents an example of simulated fields—obtained using the DLR's in-house Matlab toolbox PILab—in the uplink and downlink, where it is readily seen the different aspects influencing the propagation of optical waves in ground-GEO scenarios. On the one hand, for the uplink channel the beam size at the GEO satellite is in the order of a few hundred meters to a few kilometers, which is much larger than the probable size of the receiving aperture diameter on the satellite–in the order tens of centimeters. This situation clearly puts the uplink scenario in the theoretical limit of the point receiver case, as the beam spatial coherence length is much larger than the receiver size. The expression for the uplink SI, considering a point receiver, is given by [31]

$$\sigma_I^2 = \exp\left[\frac{0.49\sigma_{I_{\mathrm{Bu}}}^2}{\left(1+0.56(1+\Theta)\sigma_{I_{\mathrm{Bu}}}^{12/5}\right)^{7/6}} + \frac{0.51\sigma_{I_{\mathrm{Bu}}}^2}{\left(1+0.69\sigma_{I_{\mathrm{Bu}}}^{12/5}\right)^{5/6}}\right] - 1, \tag{7}$$

where Θ is a parameter describing the beam phase front radius at the receiver plane and $\sigma_{I_{\mathrm{Bu}}}^2$ is the uplink Rytov variance for Gaussian beams, which depends directly on the selected C_n^2 profile model and their corresponding expressions can be found in [31, Ch. 12]. Note that the expression given in (7) assumes that the beam is being tracked—i.e. no beam wander effects are included.

On the other hand, in the downlink case the receiving telescope can be built to have an aperture size of several tens of centimeters, or even in the 1 m range, which is larger than the speckle sizes produced by the atmospheric turbulence in the downlink, and thus the intensity fluctuations can be averaged by the receiving aperture (See Figure 3). The scintillation index in the downlink, including the receiver aperture averaging effects, can be calculated through Eq. (39) in [31, Ch. 12].

For most of the OGEOFL scenarios of practical interest—i.e. links of about 30° elevation angle or larger—the irradiance data at the receiver, either in the downlink or uplink channel, can be modeled by means of the Lognormal (LN) probability density function (PDF).

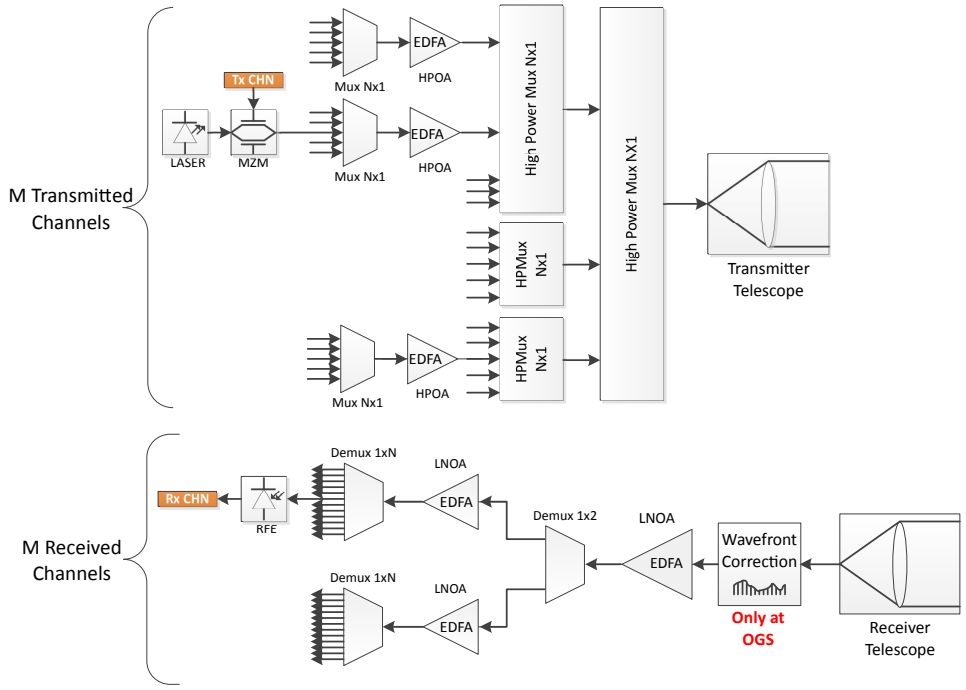

Figure 4: Schematic for a typical implementation of a OGEOFL DWDM transmitter (top) and receiver (bottom). Wavefront correction is only needed at the OGS to increased turbulence-degraded fiber coupling efficiency.

3 OGEOFL Transmission schemes options

Optical GEO feeder links technology, once implemented, would able to transmit very high data rates up to the order of several Terabits per second by making use of wavelength division multiplexing schemes, to support high throughput satellite systems in the midterm future [6]. To achieve Terabit/s capacity in future OGEOFL, a number of optical channels—in the order of a few hundreds—operating at multi-Gigabit/s rates are multiplexed to be launched through a single telescope, and this approach requires the implementation of DWDM technology. Nevertheless, this kind of foreseen ultra-high capacity depends on the availability of DWDM space-qualified optoelectronics as addressed in Section 2.1.

In the upper part of Figure 4 the schematic of a DWDM transmitter is presented, while in the lower part the receiver is shown. At the transmitter, different data stream signals are used to modulate a laser source tuned to an optical DWDM channel, where the data stream can correspond to a single signal or a multiplex. Next, all optical carriers are multiplexed into a single fiber in order to inject them into a high power optical amplifier. The optical multiplexing most likely will be executed in cascaded stages, to better handle the high powers resulting from multiplexing hundreds of wavelengths. First, a few wavelengths will be optically amplified by a single high power Erbium doped fiber amplifier (EDFA), operating as a high-power optical amplifier (HPOA). Finally, all the outputs, to be launched through the transmitting telescope, should be combined using multiplexers based on refractive optics—in order to cope to the high aggregate power.

In the lower part of Figure 4, the schematic of a DWDM receiver is presented. After collection of the incoming optical data-carrying signal by a receiving telescope, the light is coupled into a single mode fiber (SMF) to then pass through an EDFA operating as a low noise optical amplifier (LNOA). Next, the signal in optically demultiplexed—in one various stages—to obtain the individual carrier wavelengths. Finally, the optical signals are converted to the electrical domain, through the receiver front-end (RFE), composed by a photodetector (e.g. a PIN or APD), and an electrical pre-amplifier and filter. Thus, recovering the initially transmitted data stream.

In order to reach the Terabit/s capacity HTS systems with RF technology a rather high number of gateway stations are needed, while a single optical GW can cope with such capacity. Nonetheless, optical ground stations are prone to cloud blockage and to achieve carrier-class availability location diversity is needed for the deployment of an OGS network. Figure 5 presents a comparative example between optical and RF approaches, where the assumptions for the RF feeder link are: 200 beams with full frequency reuse of 1, modulation order 16, 2/3 code rate, 10 % roll-off factor and 2 polarizations. Distances between the different optical GWs must be large enough to guarantee a complete weather decorrelation between the sites of the network, such that if one OGS is covered by clouds another one most likely will have clear sky conditions [7]. In order to reach a 99.9 % availability in terms of cloud coverage, about 10 optical GWs are required in an OGS network that includes continental Europe, North of Africa and the Canary Islands [8]. In order to achieve the best possible link stability, the satellite telescope needs to be equipped with a pointing assembly. Thus, procuring a seamless handover between two GW stations, the satellite requires a pair of aerial optical terminals to implement macro diversity against cloud coverage.

In the following, it is assumed that the information to be transmitted by the OGEOFL is a DVB-S2X signal [11],

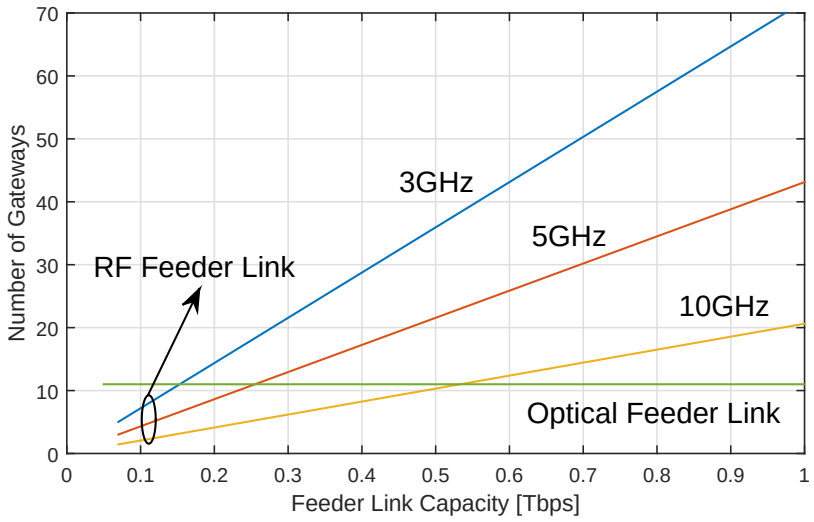

Figure 5: (Color online) Number of GWs vs. feeder link capacity comparison between optical and RF alternatives for the uplink transmission carrier [36]. RF feeder link assumes all spectrum usage in Ka band (blue line), Ka+Q/V band (red line) and Q/V+W band (yellow line). OGEOFL (green line) can provide Terabit capacity with only one OGS. To achieve an availability of 99.9 % about 10 optical GWs are needed.

which is an extension of the DVB-S2 standard [10], which allows for TV broadcasting, Internet access and professional services, such as digital news gathering [35].

Optical transmission from the OGS to the satellite can be performed by two approaches: transparent—i.e. only amplify and forward onboard—or regenerative where (de)modulation and/or (de)coding are performed onboard. The typical communication satellite operates on a Bent Pipe principle where only amplification and conversion between uplink and downlink frequency are applied, which is the preferred architecture by satellite telecom operators for its transparency to modulation and coding and relative low complexity. In an optical GEO feeder link scenario, when implementing either transparent or regenerative option, the satellite design needs to include an optical payload for the reception and processing of the laser data-carrying signal, which would replace the RF feeder link receiver in comparison with pure RF feeder link system. A transparent OGEOFL can actually be implemented in analog mode, where the DVB-S2X signal directly modulates a laser source in the GW, or in digital mode, where RF signal is sampled and transmitted as bits optically to the satellite.

3.1 Analog Transparent Option

In the analog transparent transmission scheme the basic architecture is the same as the one presented by numerous reports on the transmission of wireless RF services over FSO [37, 38, 39, 40, 41, 42]. This architecture employs an intensity-modulation direct-detection (IM/DD) scheme, which directly modulates the optical carrier with the output RF signal from the DVB-S2X chain at the GW. Thus, the data-carrying laser beam is transmitted through the turbulent atmosphere—and disturbed by IRT—to the GEO satellite where the signal is then collected by a telescope, optically pre-amplified by means of a low noise optical amplifier (LNOA), and finally converted by a square law optoelectrical detector to recover the original DVB-S2X RF signal. In this scheme, the intermediate frequency (IF) for the uplink RF signal shall conveniently be selected in order to minimize the impact on the satellite's RF payload.

The requirements imposed by the link budget in the optical GEO uplink channel force the use of high optical power amplifiers at the GW transmitter, thus making the analog signal prone to degradation due optical nonlinearities in the amplifier. This might have some impact on the RF signal quality, and ultimately on the signal-to-noise ratio (SNR) at the satellite uplink receiver. It is expected that optical powers needed for the uplink are in the order of tens of watts per wavelength [6, 43]. Current DWDM high power optical amplifier technology can provide off-the-shelf maximum saturated output power up to 10 W [44], while single wavelength amplifiers can go up to about 40 W [45]. Depending on the specific link conditions, it might be possible that one amplifier is used for a single channel, and thus the initial multiplexing stage of the transmitter scheme shown in Figure 4 is not necessary. In the downlink, a few watts per wavelength should be enough to provide a good signal-to-noise ratio at the OGS receiver.

3.2 Digital Transparent Option

Another possibility to implement an OGEOFL keeping the transparency requirement is by transmitting a digitized version of the DVB-S2X RF signal generated at the GW [46, 7]. With this approach the DVB signal is converted from analog to digital domain, by means of a decomposition of the baseband signal in its real (in-phase) and imaginary (quadrature) components [6]. As an example, consider a signal, arriving at the GW at L RF-band, composed of 3 carriers and 1.45 GHz of aggregate bandwidth, that are downconverted to baseband and de-multiplexed. Next, each

carrier is sampled at 6-bit resolution per dimension of the complex signal, resulting in a 37 dB signal-to-distortion ratio (SDR) and a 12x bandwidth expansion factor [6].

Current technology for high-speed analog-to-digital (ADC) and digital-to-analog (DAC) converters can offer conversions in the Gigasample/s domain [47], which is considered sufficient—even taking into account the oversampling factor needed to accurately quantize the analog signal [6]. Nevertheless, high-speed ADCs and DACs need first to be qualified for space operation, before the digital transparent OGEOFL scheme becomes a viable option. When the digitized version of the DVB baseband signal is received, the GEO satellite demodulates the optical signal and uses the samples to reconstruct the original RF signal, so it can be transparently processed by the satellite RF payload and be sent through the downlink chain to the end user.

The digital option offers a more robust implementation against fading events in the atmospheric turbulent channel as compared to the analog option, since the transmission allows for the application of digital signal processing algorithms, at the expense of increased satellite complexity, an onboard processor is needed to reconstruct the RF signal. Additional robustness against burst errors can be achieved by protecting the digital samples using forward error correction (FEC) coding, specifically designed to compensate IRT adverse effects, for protection against deep and long fades events—in the order of milliseconds—in the atmospheric optical channel [6]. The implementation of IRT-FEC results in processing requirements of about 20 Gbps that have been demonstrated elsewhere [48]. Nevertheless, hardware expansion and parallelization of the processing is mandatory to cope with the overall capacity of a Terabit/s throughput GEO satellite [6]. On the other hand, considering the long fades inherent to the optical turbulent channel, onboard memory in the order a few GByte is required for the interleaver size.

The transmission of the digitized version of the DVB signal can be made either with IM/DD or coherently, as the uplink optical source is transmitting bits. IM/DD supports transmitter diversity allowing for an increased transmitted power and reduced IRT-fading due to scintillation at the receiver plane on the satellite. In coherent modulation, all the necessary power in the uplink must be transmitted through a single telescope, as weakly correlated multiple sources in a transmitter diversity scheme would randomly interfere with each other destroying the phase-conveyed information. It is noteworthy that this type diversity is implemented only for IM/DD modulation schemes to counter attack the adverse effects of atmospheric turbulence, and the spatial separation needed between optical sources should be at least in the order of the Fried parameter (3).

3.3 Digital Regenerative Option

The most robust option, in terms of IRT-induced fading, in optical GEO satellite architectures is when onboard digital regeneration capabilities are implemented, that is when all data transmitted through the atmospheric optical uplink channel is in digital form allowing for the use of protection and correction schemes. In this digital regenerative (DR) transmission scheme, the original baseband bit stream is directly transmitted through the optical carrier. As transmission of data in the optical feeder uplink is done in baseband some operations traditionally performed in the GW are now executed onboard the satellite, and thus the effect of fading in the feeder uplink has the least impact in the user terminal. Nevertheless, this improved performance against fading comes with the price of notably increased satellite design complexity and transparency is no longer possible. In reality, the regenerative payload for a Terabit/s class satellite is extremely challenging to be realized in practice due to power, mass and accommodation constraints. Additionally, the satellite flexibility to adapt to new changes in the DVB format, which might appear in future revisions of the standard, is lost once the satellite has been launched. Digital regenerative schemes can be performed with two different options, namely soft and fully regenerative.

In the DR soft option, the baseband (BB) data bit frames with the DVB-S2X FEC coding, which can be additionally protected against fading by an IRT-FEC, are transmitted over the optical carrier through the atmospheric turbulent channel and received by the optical payload onboard the satellite. Once data is recovered in the electrical domain, the IRT-FEC is decoded to correct for errors introduced by the atmospheric fading channel, the BB frames can be processed onboard by the remainder of the DVB chain with the corresponding amplitude and phase modulation, as well as the baseband filter—i.e. pulse shaping. The FEC-protection of the optical links requires interleaver depths in the orders of 100 ms, causing according delay issues. Onboard robust processing capability is required for this FEC-decoding translating into an impact on payload complexity, mass and power consumption.

The fully DT regenerative option is similar in concept to the soft regenerative option, as the BB frames are also transmitted over the optical carrier, but the DVB-S2X FEC coding and modulation blocks are included in the satellite RF chain to achieve most robust system against bit error-rate. Similarly, an additional IRT-FEC code can be applied to the BB frames, to be transmitted from the GW to the satellite through the optical uplink channel, in order to protect the data against the IRT-induced fading. Evidently, the inclusion of specific blocks of the DVB data processing chain at the satellite considerably increases the architecture complexity, and the possibility of transparency—even the quasi Bent Pipe architecture, as in the digital transparent option—is completely lost.

3.4 Discussion on transmission schemes complexity

Figure 6 shows a diagram with the trade-off between the different alternatives, presented in above, to implement an optical GEO feeder link for HTS in terms of satellite complexity and their robustness against fading events. In the lower left part of the chart appear the transparent options—both analog and digital—that are the ones allowing for

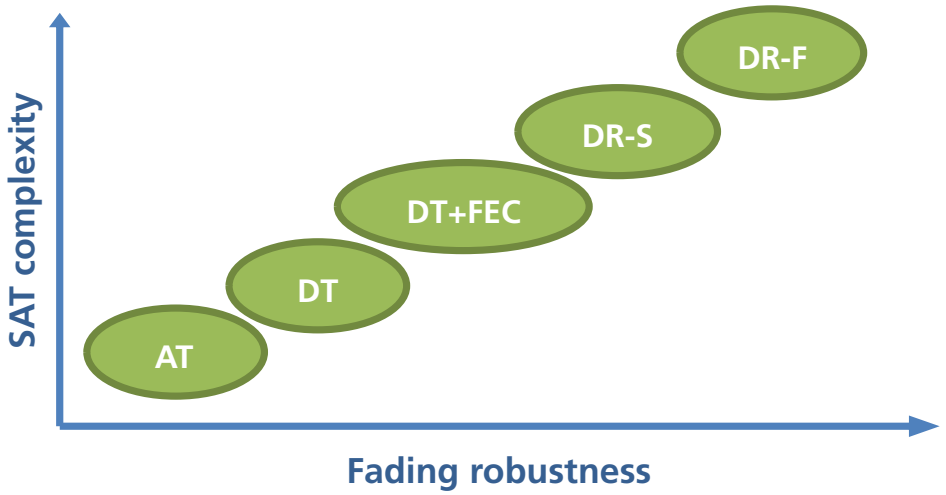

Figure 6: (Color online) Satellite complexity vs. Fading robustness of different Optical GEO feeder link schemes. AT: Analog Transparent, DT: Digital Transparent, DR: Digital Regenerative, S: Soft, F: Full, FEC: Forward Error Correction.

maximum flexibility in the satellite architecture and least complexity. Nevertheless, these are the options that offer the least robustness against atmospheric index of refraction turbulence fading protection, which is one of the major impediments for the deployment of OGEOFL technology. Conversely, in the upper right zone of the chart alternatives with improved error correction capabilities are grouped, which come at the expense of increasing satellite complexity and loss of flexibility.

As it is readily seen in Figure 6, the middle of the chart holds the digital transparent plus FEC option. This represents a fair compromise between transparency/complexity of the GEO satellite and the robustness against IRT-fading imposed by the optical uplink channel. On the one hand, all the convenience of transmitting data in digital format are gained—versus the analog transparent option—and transparency is still maintained at the satellite, while the architecture complexity is moderately increased by the necessity of introducing high-speed digital-analog converters and onboard processing to decode the IRT-FEC protected digital samples of the original DVB-S2X signal that has been generated at the GW. Nevertheless, the analog transparent option seems to be more attractive for satellite telecom operators in the short-term due to the minimal impact on the satellite payload design, and it might very well be the option chosen for the first HTS systems making use of optical GEO feeder link technology. The major drawback for the AT option is the poor protection against turbulence-induced long fade events, which translates into outages of the service. Therefore, extensive work should be done in this field—studying in detail the adverse effects of atmospheric turbulence over non IRT-FEC-protected data—to assess if carrier-class availabilities are possible.

The following section only deals with the analog and digital transparent options presented in Section 3.1 and Section 3.2, respectively.

4 Link Budget

When calculating a link budget for a GEO feeder link scenario, which employs optical technology to transmit data, many aspects need to be taken into account. All the different elements playing a role in the link budget calculation are depicted in Figure 7, where all major loss sources for the optical channel are included, along with the different elements from the OGS and GEO satellite payload involved in the estimations. Figure 7 is focused on the feeder uplink channel for the analog transparent option discussed above, and the dashed lines and blocks refer to additional elements corresponding to the digital transparent option for optical GEO feeder links.

The calculation of the available signal-to-noise ratio (SNR) becomes essential when assessing if the link is feasible, for the specific scenario conditions. The SNR expression at the receiver output is

$$\mathrm{SNR} = \frac{i_{\mathrm{S}}^2}{\sigma_{\mathrm{S}}^2 + \sigma_{\mathrm{B}}^2 + \sigma_{\mathrm{S-ASE}}^2 + \sigma_{\mathrm{ASE-ASE}}^2 + R_I^2 \mathrm{NEP}^2 B_{\mathrm{S}}^2}, \tag{8}$$

where $i_{\mathrm{S}} = R_I P_{\mathrm{T}}$ is the generated signal photocurrent, for a received optical power P_{T}; σ_{S}^2 is the shot noise associated to the received signal, σ_{B}^2 is the noise coming from the background optical power, R_I is the photodetector current sensitivity, B_{S} is the bandwidth of transmitted signal—i.e. it is assumed that an electrical filter matching the signal bandwidth is present at the output of the RFE—and NEP is the noise equivalent power that characterizes the noise figure of the photodetector.

The process that detects the photons impinging on the optical detector's surface is described by the occurrence of independent random events, modeled by the Poisson distribution. This randomness in the photo-detection process is

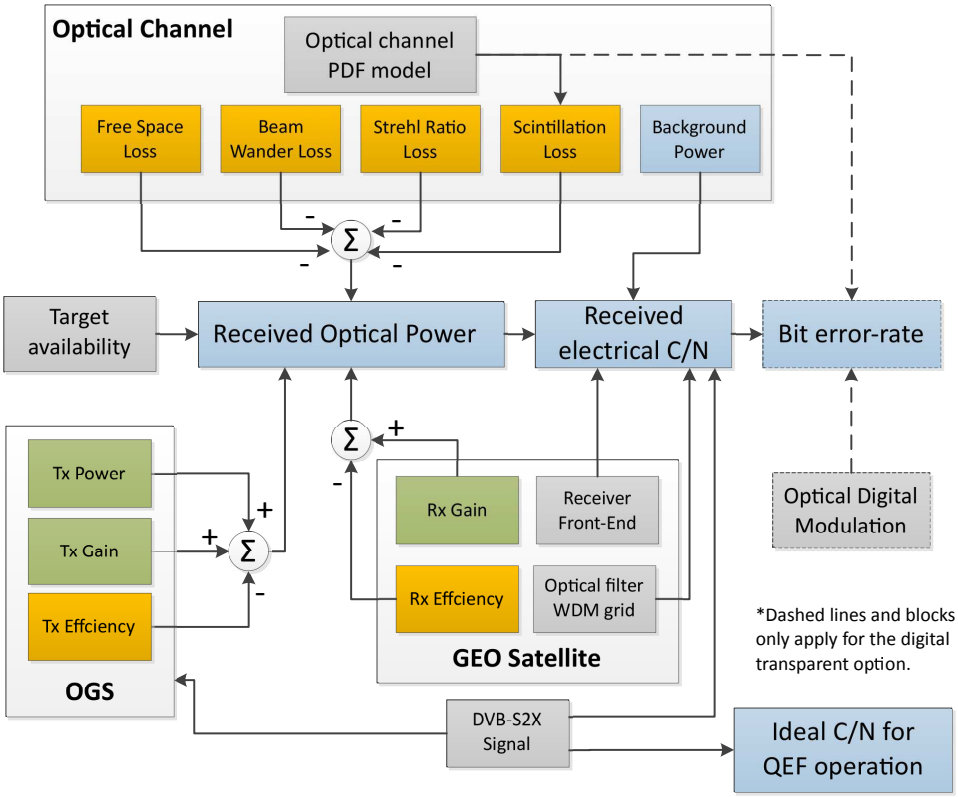

Figure 7: (Color online) Schematic representation of optical GEO feeder link budget. Losses are indicated in yellow, gains in green, inputs in gray and outputs in blue.

what gives rise to the shot and background noises, which are given by

$$\sigma_{\mathrm{S}}^2 = 2eR_I P_{\mathrm{S}} M F B_{\mathrm{S}},\ \sigma_{\mathrm{B}}^2 = 2eR_I P_{\mathrm{B}} M F B_{\mathrm{S}}, \tag{9}$$

respectively; where e is the electron charge, M is the photodetector intrinsic gain, P_{S} is the average received optical power, P_{B} is the background optical power, and F the excess noise factor. For a PIN photodiode intrinsic the gain and the excess noise factor are unity.

As the optical receiver is composed by an EDFA pre-amplifier, in the SNR calculation additional noise sources need to be considered. At the output of the EDFA, the input signal is amplified by a gain factor G and the EDFA output noise called amplified spontaneous emission (ASE) is added. The ASE noise is modeled as a white noise with power spectrum density of $N_{\mathrm{ASE}} = (G-1)h\nu n_{\mathrm{sp}}$, where n_{sp} is the population inversion factor related to the EDFA noise figure NF by $n_{\mathrm{sp}} = \mathrm{NF}/2$ [49]. Moreover, h is the Planck constant and ν is the center frequency at 1550 nm. After filtering by the optical filter B_o, the ASE noise is modeled as a white noise limited to the $[-B_o/2, +B_o/2]$ frequency spectrum. The optical filter bandwidth is generally larger than the electrical filter bandwidth due to the difficulty to achieve very narrow filters in the optical domain. Thus, noise produced by the interaction between the signal and the ASE noise $\sigma^2_{\mathrm{S-ASE}}$, and the interaction between the ASE and itself $\sigma^2_{\mathrm{ASE-ASE}}$ is given by [49]

$$\sigma_{\mathrm{S-ASE}}^2 = 4R_I^2 G P_{\mathrm{S}} N_{\mathrm{ASE}} B_{\mathrm{S}},\ \sigma_{\mathrm{ASE-ASE}}^2 = 4R_I^2 N_{\mathrm{ASE}}^2 B_{\mathrm{S}}(2B_o - B_{\mathrm{S}}). \tag{10}$$

Finally, in order to calculate σ_{B}^2 the total background optical power must be estimated. The total background radiation can be characterized by the spectral radiance of the sky that depends on the elevation angle, and changes for day and night operation. In nighttime, the sky emissivity for a nearly horizontal path through the atmosphere is essentially that of a black body radiating at the temperature of the lower atmosphere. The behavior for daytime conditions will be very similar to that of nighttime, with the corresponding change due to higher temperatures, and the addition of scattered sun radiation below 3 μrad [50]. Once the spectral radiance of the sky N_{B} is known, the total optical power at the receiver, due to background, can be calculated as

$$P_{\mathrm{B}} = N_{\mathrm{B}} \left(\pi \frac{D_{\mathrm{R}}}{2} \frac{\mathrm{FOV}}{2}\right)^2 B_o \eta_{\mathrm{R}}, \tag{11}$$

where B_o is the optical bandwidth of the receiving telescope, which will be dependent of the DWDM grid chosen for the OGEOFL, and FOV is the detector's field of view that is determined by the telescope focal length and the diameter of the SMF core.

In the next two sections, it is shown how to calculated the received optical power in optical GEO feeder link scenario, both in the uplink and downlink directions.

4.1 Feeder uplink received power

The expression for the received average optical power P_{R}, in the uplink direction, detected at distance L is given by

$$P_{\mathrm{R}} = P_{\mathrm{T}} G_{\mathrm{T}} \eta_{\mathrm{T}} \tau_{\mathrm{ATM}} L_{\mathrm{FS}} L_{\mathrm{SR}} L_{\mathrm{BW}} L_{\mathrm{SI}} G_{\mathrm{R}} \eta_{\mathrm{R}} \eta_{\mathrm{F}}, \tag{12}$$

where P_{T} is the average power transmitted by the OGS laser source, through an aperture diameter D_{T};

$$G_{\mathrm{T}} = \left(\frac{\pi D_{\mathrm{T}}}{\lambda}\right)^2, \quad G_{\mathrm{R}} = \left(\frac{\pi D_{\mathrm{R}}}{\lambda}\right)^2, \tag{13}$$

are the OGS transmitter and GEO satellite receiver gains, respectively; η_T and η_R are the transmitter and receiver efficiencies, respectively; τ_{ATM} is the atmospheric attenuation, as given in (1); $L_{\mathrm{FS}} = (\lambda/4\pi L)^2$ is the free-space loss. The extra spread loss L_{SR}, due to atmospheric turbulence, is given in terms of the Strehl ratio given in (5), and

$$L_{\mathrm{BW}} = \exp\left(-G_{\mathrm{T}} \theta_{\mathrm{BW}}^2\right) \tag{14}$$

corresponds to the beam wander loss [51], defined in terms of the angular beam wander θ_{BW} defined in Section 2.4.

Additionally, the the scintillation loss L_{SI} in decibels is defined as [52]

$$L_{\mathrm{SI}} = \left(3.3 - 5.77\sqrt{\ln \frac{1}{p_{\mathrm{thr}}}}\right) \sigma_I^{4/5} \,[\mathrm{dB}], \tag{15}$$

where σ_I^2 is the SI value for the uplink given in (7), and p_{thr} defines the target outage probability of the link. Note that (15) assumes that the statistics of the irradiance data at the receiver are governed by the Lognormal distribution.

Finally, the SMF coupling efficiency under atmospheric turbulence is [53]

$$\eta_{\mathrm{F}} = 8a^2 \int_0^1 dx_2 \int_0^1 dx_1 \, \exp\left[-\left(a^2 + \frac{D_{\mathrm{R}}^2}{4\rho_0^2}\right)(x_1 + x_2)^2\right] I_0\left(\frac{D_{\mathrm{R}}^2}{2\rho_0^2} x_1 x_2\right) x_1 x_2, \tag{16}$$

where $a = \pi D_{\mathrm{R}} W_m/(2\lambda F)$, W_m is the field radius of the fundamental mode that propagates through the SMF (usually about 5 μm), F is the focal length of the receiving telescope, and $\rho_0 = 0.48 r_0$ is the atmospheric coherence radius—which is directly related to the Fried parameter give in (3).

In the uplink direction, as shown in Figure 3, the turbulent structures defined by ρ_0 are much larger than the probable size of the GEO satellite receiving aperture—i.e. $\rho_0 \gg D_{\mathrm{R}}$. Consequently, the maximum fiber coupling efficiency $\eta_{\mathrm{F}} = 0.815$ can be obtained when $a = 1.12$, which can be achieved through careful design of the receiving telescope by manipulating the D_{R}/F ratio.

4.2 Feeder downlink received power

The expression for the received average optical power P_{R}, now in the downlink direction, is given by

$$P_{\mathrm{R}} = P_{\mathrm{T}} G_{\mathrm{T}} \eta_{\mathrm{T}} \tau_{\mathrm{ATM}} L_{\mathrm{FS}} L_{\mathrm{SI}} G_{\mathrm{R}} \eta_{\mathrm{R}} \eta_{\mathrm{F}}, \tag{17}$$

where P_{T} is now the average power transmitted by the GEO satellite laser source, through an aperture diameter D_{T}; G_T and G_R are the GEO satellite transmitter and OGS receiver gains, respectively. With respect to (12), L_{SR} and L_{BW} losses are not included in the downlink case, as these are exclusive of the uplink scenario. Finally, the fiber coupling efficiency is estimated by using (3) in (16).

4.3 BER calculation for DT option

When transmitting the digitally sampled version of the DVB signal, there is a considerable expansion in the required bandwidth due to the quantization factor. The actual signal rate to be transmitted in the DT option is given by $R_{\mathrm{S_{DT}}} = 2R_{\mathrm{S}}N_b$, where R_{S} is the original DVB signal rate in symbols/s, N_b is the sampling resolution in bits/symbol and the factor 2 accounts for I and Q components. In the DT option the sampled bits of the DVB RF-baseband signal, for the I and Q components, are multiplexed into a single bit stream. When more than one RF-subcarrier is to be transmitted, its digital samples are also multiplexed in the same bit stream.

The quantization of the RF-subcarrier waveform introduces a distortion that will affect the SNR. The signal-to-distortion ratio (SDR) in decibels, due to quantization noise, is given by

$$\mathrm{SDR} = 6.02N_b + 1.76 \,[\mathrm{dB}]. \tag{18}$$

This implies that the recovered signal SNR—after the digital-to-analog conversion process in the receiver—is always upper bounded by the SDR, which for example is about 37 dB when a 6 bit resolution DAC is used.

Additionally, the bit error-rate (BER) can be estimated for the selected modulation format. In the presence of optical turbulence, the probability of error is a conditional probability owing to the random nature of the received

optical power. Thus, the SNR becomes a random variable and consequently the BER (or symbol error-rate) has to be averaged over all possible received optical signal levels, according to the fading PDF model. This yields

$$\mathrm{BER}(\sigma_I^2) = \int_0^\infty f_I(I;\sigma_I^2) P_b(I) dI,\ I > 0, \tag{19}$$

where $P_b(I)$ is the bit-error probability of a given modulation, $f_I(I;\sigma_I^2)$ is the lognormal PDF that models the IRT process, and σ_I^2 is the scintillation index that measures the turbulence strength.

When transmitting the digitized version of the original DVB-S2X RF signal a target BER is set, which if met guarantees the recovering of the signal with a SNR only limited by the SDR due to the quantization process. In the following, the target BER $\leq 10^{-9}$ is set to assess if the OGEOFL closes the link budget for the DT option, corresponding to the frame-error rate (FER) target of DVB-S2X.

Additional protection of the transmitted signal against IRT-induced fades can be achieved with the use of a FEC, as discussed in Section 3.2. A possibility for such a code could be the well-known Reed-Solomon (RS) error correction code, although other type of codes are also possible [6]. If the assumption that an infinitely long interleaver is available—i.e. the fade correlation time is negligible—a (n, k) RS code is capable of correcting $t = \lfloor (n-k)/2 \rfloor$ symbols, presents a word error-rate P_w lower bounden by [54]

$$P_w = 1 - \sum_{i=0}^{t} \binom{n}{i} P_s^i (1-P_s)^{n-i}, \tag{20}$$

where $P_s = 1 - (1-P_b)^m$ is the symbol error-rate, $m = log_2(n-1)$ and P_b is the BER—averaged over the turbulent channel—given by (19). Moreover, the BER lower bound for the RS code is $P_{blow} = P_w t/(nm)$.

In the following a $(255, 239)$ RS code will be used to estimate the effects of using an IRT-FEC, when transmitting OOK modulated data in the OGEOFL.

4.4 Scenarios

In this section link budget calculations are presented for the uplink direction to assess the viability of the implementation of GEO feeder links based on optical technology. For the calculations some scenarios parameters need to be defined. The IRT turbulence is modeled with the C_n^2 profile given in (2), with $A = 1.7 \times 10^{-14}\mathrm{m}^{-2/3}$, and a 3 dB cloud margin for thin cirrus clouds is assumed [55]. Also, the scintillation index loss calculation is done for a 99.99 % availability.

On the GEO satellite, it is assumed that the spacecraft is located at 9 °E, a 25 cm receiving telescope with an optical filter of 0.8 nm—i.e. corresponding to a DWDM grid of 100 GHz—is present. The receiver optical chain has an 30 dB EDFA pre-amplifier, with 4 dB noise figure. The photodetector is a PIN diode of 20 GHz electrical bandwidth, 0.75 A/W responsivity, and NEP = 2.5 pW/$\sqrt{\mathrm{Hz}}$.

For the OGS two locations are selected. Firstly, the ESA OGS in Tenerife is the natural selection for a site to serve in a first OGEOFL demo, which is located at approximately at 2300 m above m.s.l., and secondly, Madrid at 667 m above m.s.l. as it is a potential site for deployment of a future OGS network, thanks to its proximity to the fiber optics European backbone [9].

Table 1 presents all the link budget calculations for the two different OGS locations selected, for the AT and DT transmission schemes options, and it is divided in six sections each presenting different information. In the first section the OGS transmitter power is shown, along with the transmitter telescope diameter and divergence. Here, the optimum aperture size to minimize the link loss is always used for each scenario. The second section of the table gives the value of the various atmospheric parameters that play a role in the link budget calculation. Also, the Greenwood frequency is given so the link designer can estimate the size of interleaver if IRT-FEC is to be implemented. The size of the interleaver depends on the mean correlation time of the atmospheric channel, which is the inverse of the Greenwood frequency. The third section of the table shows the actual link budget calculations. The next section presents the results for the AT option, where the SNR is measured at the output of the receiver chain of the GEO satellite. The last two section in Table 1 correspond to the performance of the DT option, where the power needed to reach a BER $\leq 10^{-9}$, is shown, assuming OOK modulation. Additionally, three DVB signals are considered for each transmission in each location, which go from lower to higher bandwidths. A lower bandwidth signal, with 35 MHz (Signal A), is chosen because is a typical example of current DVB-S2 signals [12]. Moreover, two signal of 225 MHz (Signal B) and 450 MHz (Signal C) are chosen as they can make use the new capabilities of DVB-S2X to handle higher data rate signals. All considered signals are assumed to have a 5 % roll-off factor [12].

In order to accommodate the RF waveforms on the optical carrier, a certain dynamic range of the laser source in terms of peak-to-average optical power is required. In the AT option, the optical dynamic range should be half the number in decibels of the peak-to-average-power ratio (PAPR) of the pulse-shaped DVB-S2X modulation formats due to the assumption that the RF power is proportional to the square of the optical power. However, since the PAPR of high order modulation, e.g. up to 256-APSK, with pulse shaping is considerable and expected to be far greater than the dynamic range of practical laser sources, distortions similar to the ones in the high-power amplifier (HPA) onboard will be present, which can only be avoided by the use of a large power back-off and penalty in the power efficiency. On the other hand, for the DT option, as the modulation chosen is OOK, the peak power of the optical source should

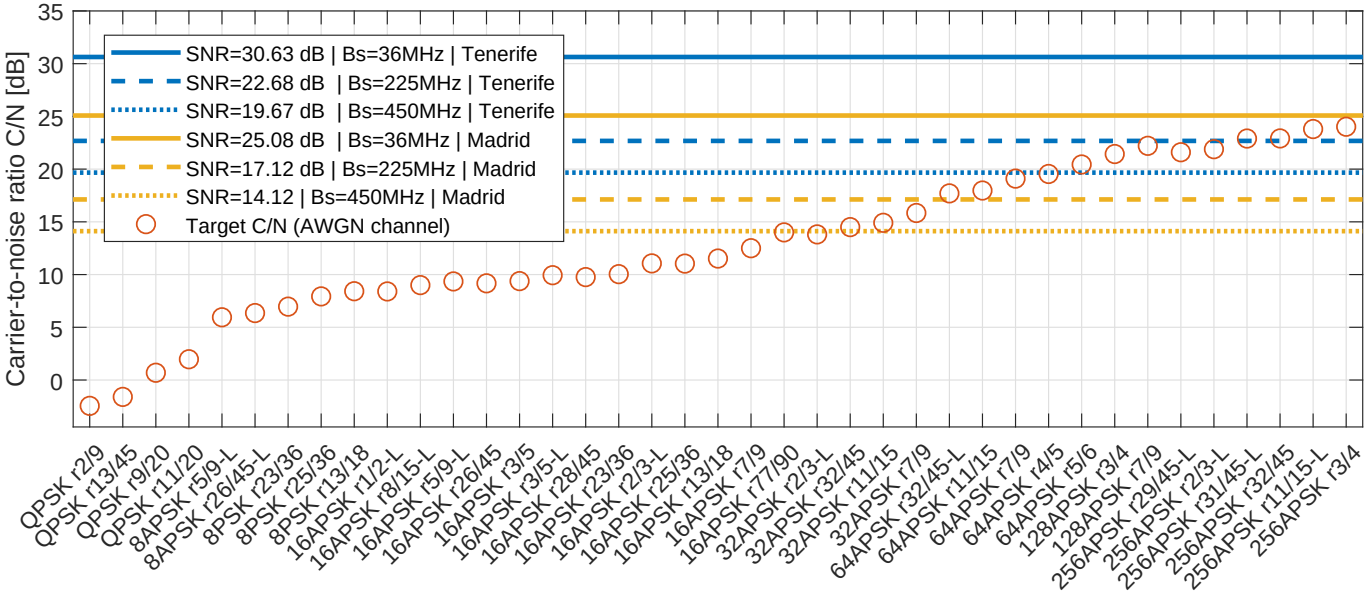

Figure 8: (Color online) Target symbol SNR (circles) for different DVB-S2X MODCODs [12], and available SNR for two different locations, namely (blue lines) Tenerife and (yellow lines) Madrid. The DVB signals analyzed correspond to those in Table 1, with bandwidths 35 MHz (solid line), 225 MHz (dashed lines) and 450 MHz (dotted lines).

be twice of the average power requirements shown in the two last sections of Table 1. Keeping the former in mind, and that current high power optical amplifiers technology can offer up to about 50 W at 1550 nm, and possibly in the mid-term future booster amplifier might reach the 100 W, some scenarios in Table 1 cannot meet the link budget for the required transmitter power with realistic values, and thus they appear with an em-dash.

In order to further analyze the results presented in Table 1, the available SNR in the AT option is compared against the target symbol SNR for a rather large set of MODCODs, supported by the DVB-S2X standard [12]. Figure 8 shows the required symbol SNR for several modulation order, ranging from QPSK to 256-APSK, and various code rates. The available SNR, in the AT option, for all the scenarios studied are shown a horizontal lines, indicating that all the MODCODs that are below any of such lines can be reliable transmitted for the corresponding scenario. Starting with the location Tenerife, using a fixed Tx power level, it is readily seen that for Signal A the link budget for all MODCODs can be closed, while for Signal B and C MODCODs up to 128-APSK and 64-APSK work, respectively. On the other hand, for location Madrid all three signals can be reliably transmitted for MODCODs up to 32-APSK, while Signal B and C only supports MODCODs up to 32 and 16-APSK, respectively.

Note that for DT option, if the BER target is met, all MODCODs are expected to work, as the recovery of the original sampled waveform is then going to be only limited by the SDR—that in this example is 37 dB, for 6 bits per dimension, which is considered to be enough for reliable transmission of the DVB-S2X signal. Moreover, the RS code used in this section, for the calculations of the DT option, is generally not the optimal FEC code for counter attacking the adverse effect of the IRT-turbulence. More optimal codes could be applied to improved the protection against burst errors due to long fade event in the atmospheric channel, and relax the power requirements to allow for more locations and atmospheric conditions to be suitable for deployment of OGS in OGEOFL [6].

5 Conclusions

This work presented an introduction to optical GEO feeder link technology. Starting from the motivation for future high-throughput satellite systems, and the payload characteristics in the mid-term future. Moreover, a framework is given covering the characteristics and implications of transmitting a data-carrying optical signal through the turbulent atmospheric channel in the uplink direction. In addition, a methodology to calculate the link budget for ground-to-GEO satellite links has been presented. Although this work is focused on the uplink channel, the downlink channel has also been addressed for completeness.

Additionally, a number of techniques to encapsulate a DVB-S2X RF signal over an optical carrier were presented. The most promising techniques, for mid-term implementation, are the analog and digital transparent options. The AT scheme is the more attractive in terms of satellite transparency and minimum impact on satellite complexity. Although the DT option imposes an increase in satellite complexity due to the need of onboard digital processing capabilities, it presents an attractive alternative thanks to the possibility of protecting the transmitted data with FEC codes efficiently designed to mitigate the adverse effects of IRT-induced fading.

An analysis was conducted in Section 4.4 for two locations and three signal data rates—with bandwidths 36 MHz (Signal A), 225 MHz (Signal B) and 450 MHz (Signal C).When the OGS is deployed in locations with excellent optical properties, as mountaintops like the ESA OGS at Tenerife, the AT option presents itself as feasible for all DVB-S2X

MODCODs while demanding relatively low Tx power levels. For OGS sites in mid-altitude locations, such as Madrid, the AT scheme requires at least four times more Tx power to support all MODCODs—i.e. a 6 dB penalty. In terms of Tx optical power requirements, the lowest data rate signal needs an average of 20 W, which should be feasible with current EDFA amplifiers. On the other hand, the largest bandwidth signals—i.e. Signal B and Signal C—can support modulation orders up to 16-APSK with the same Tx power. One important aspect for the AT option is the fact that the laser source needs to be able to handle the PAPR requirements, for the transmitted RF modulation format and order. Such analysis—which is outside the scope of this work—is crucial to identify any link degradation due to nonlinearities introduced by the high power optical amplifier, in order to have a complete assessment of the link budget for feeder uplink channel in the AT option.

In the digital transparent option, on the other hand, it is assumed that if the target of BER $\leq 10^{-9}$ is met all DVB-S2X MODCODs can be reliably transmitted. It can readily be seen, from Table 1, that for location Tenerife the DT+FEC option can always close the link budget at relatively low Tx power levels, for all three different signals assessed. Moreover, as the PAPR in the DT scheme with OOK modulation is only a factor two, the requirements of average transmitter power can be easily met with current optical amplifiers. For location Madrid, the link budget for Signal A can also be closed. Signal B with the DT+FEC option might me feasible with future EDFAs that could offer reliable operation at a higher output saturated power regime—as it would need about 76 W peak power to close the link budget. Furthermore, even Signal C could be enable if more efficient IRT-FEC are implemented, as the RC code used in this work has not been optimized.

Finally, as the main application of OGEOFL is to enable the implementation of Tbit/s throughput satellites, it is readily seen that it would be required the multiplexing of hundreds of optical carriers to reach that goal. Taking into account the analysis carried out here, the successful implementation of optical GEO feeder links would very likely require the development of optical multiplexers based on refractive optics technology, in order to handle the high aggregate optical power in a future DWDM system reaching Tbit/s capacities.

Acknowledgements

This work has been conducted in the framework of the activity "Radio over Optical GEO Feeder Links", under ESA contract no. 4000111778/14/NL/FE. Responsibility for the contents of this document resides in the author(s) or organization(s) that prepared it, and the contents of this document does not reflect the official opinion of the European Space Agency.

References

[1] Broadband Access via Integrated Terrestrial, Satellite Systems (BATS). ICT-2011.1.1 BATS D4.1: Satellite Network Mission Requirements. *Technical Report*, European Project 2012.

[2] Viasat. Viasat-2 at a glance 2020. URL `https://www.viasat.com/sites/default/files/media/documents/770853_vs-2_2019_infographic_009_lores.pdf`.

[3] Kyrgiazos A, Evans B, Thompson P, Mathiopoulos P, Papaharalabos S. A terabit/second satellite system for european broadband access: a feasibility study. *Int. J. Satell. Commun. Network.* 2014; **32**(2):63–92.

[4] Wilcoxson D. Advanced commercial satellite systems technology for protected communications. *The 2011 Military Communications Conference*, 2011; 2280–2285.

[5] Perez-Trufero J, Evans BG, Dervin M, Baudoin C. High throughput satellite system with Q/V-band gateways and its integration with terrestrial broadband communication networks. *32nd AIAA International Communications Satellite Systems Conference*, 2014; 255–264.

[6] Dimitrov S, Matuz B, Liva G, Barrios R, Mata-Calvo R, Giggenbach D. Digital modulation and coding for satellite optical feeder links. *7th Advanced Satellite Multimedia Systems Conference (ASMS)*, 2014.

[7] Perlot N, Dreischer T, Weinter CM, Perdigues J. Optical GEO feeder link design. *Future Network & MobileSummit 2012 Conference Proceedings*, Cunningham P, Cunningham M (eds.), 2012.

[8] Poulenard S, Ruellan M, Roy B, Riédi J, Parol F, Rissons A. High altitude clouds impacts on the design of optical feeder link and optical ground station network for future broadband satellite services. *Free-Space Laser Communication and Atmospheric Propagation XXVI*, *Proc. SPIE*, vol. 8971, Hemmati H, Boroson DM (eds.), International Society for Optics and Photonics, 2014; 897 107.

[9] Poulenard S, Crosnier M, , Rissons A. Ground segment design for broadband geostationary satellite with optical feeder link. *J. Opt. Commun. Netw.* 2015; **7**(4):325–336.

[10] ETSI EN 302 307. Digital video broadcasting (DVB); second generation framing structure, channel coding and modulation systems for broadcasting, interactive services, news gathering and other broadband satellite applications (DVB-S2) March 2013.

[11] ETSI EN 302 307-2. Digital video broadcasting (DVB); second generation framing structure, channel coding and modulation systems for broadcasting, interactive services, news gathering and other broadband satellite applications (DVB-S2); part ii: S2-extensions (S2-X) March 2015.

[12] DVB Document A171-2. Digital Video Broadcasting (DVB) implementation guidelines for the second generation system for broadcasting, interactive services, news gathering and other broadband satellite applications; part 2 - S2 Extensions (DVB-S2X).

[13] Poliak J, Mata-Calvo R, Rein F. Demonstration of 1.72 tbit/s optical data transmission under worst-case turbulence conditions for ground-to-geostationary satellite communications. *IEEE Communications Letters* 2018; **22**(9):1818–1821.

[14] German Aerospace Center (DLR). Terabit-throughput satellite system technology 2020. URL `https://www.dlr.de/kn/desktopdefault.aspx/tabid-2081/6941_read-53312/`.

[15] Solomon S, Schmeltekopf AL. On the interpretation of zenith sky absorption measurements. *J. Geophys. Res.* 1987; **92**(D7):8311–8319.

[16] Fletcher G, Hicks T, Laurent B. The SILEX optical interorbit link experiment. *J. Electron. Comm. Eng.* 1991; **3**(6):273–279.

[17] Cazaubiel V, Planche G, Chorvalli V, Le Hors L, Roy B, Giraud E. LOLA: A 40000 km optical link between an aircraft and a geostationary satellite. *Sixth International Conference on Space Optics*, Wilson A (ed.), Proc. ESA/CNES ICSO, 2006; 87.1.

[18] Mata-Calvo R, Becker P, Giggenbach D, Moll F, Schwarzer M, Hinz M, Sodnik Z. Transmitter diversity verification on artemis geostationary satellite. *Free-Space Laser Communication and Atmospheric Propagation XXVI*, *Proc. SPIE*, vol. 8971, Hemmati H, Boroson DM (eds.), 2014; 897 104.

[19] Fields R, Kozlowski D, Yura H, Wong R, Wicker J, Lunde C, Gregory M, Wandernoth B, Heine F. 5.625 gbps bidirectional laser communications measurements between the NFIRE satellite and an optical ground station. *International Conference on Space Optical Systems and Applications*, 2011.

[20] Muehlnikel G, Kämpfner H, Heine F, Zech H, Troendle D, Meyer R, Philipp-May S. The alphasat geo laser communication terminal flight acceptance tests. *Proc. International Conference on Space Optical Systems and Applications (ICSOS)*, 2012.

[21] Kartalopoulos SV. *Introduction to DWDM Technology*. SPIE Press & IEEE Press, 2000.

[22] International Telecommunication Union (ITU). Recommendation ITU-R G.694.1: Spectral grids for WDM applications: DWDM frequency grid 2012.

[23] Giggenbach D, Becker P, Mata-Calvo R, Fuchs C, Sodnik Z, Zayer I. Lunar optical communications link (locl): Measurements of received power fluctuations and wavefront quality. *Proc. International Conference on Space Optical Systems and Applications (ICSOS)*, 2014.

[24] Sans M, Sodnik Z, Zayer I, Daddato R. Design of the ESA optical ground station for participation in LLCD. *Proc. International Conference on Space Optical Systems and Applications (ICSOS)*, 2012.

[25] Sodnik Z, Smit H, Sans M, Zayer I, Lanucara M, Montilla I, Alonso A. Llcd operations using the lunar lasercom ogs terminal. *Free-Space Laser Communication and Atmospheric Propagation XXVI*, *Proc. SPIE*, vol. 8971, Hemmati H, Boroson DM (eds.), 2014; 89 710W.

[26] Sodnik Z, Smit H, Sans M, Giggenbach D, Becker P, Mata-Calvo R, Fuchs C, Zayer I, Lanucara M, Schulz KJ, *et al.*. Results from a lunar laser communication experiment between NASA's LADEE satellite and ESA's optical ground station. *Proc. International Conference on Space Optical Systems and Applications (ICSOS)*, 2014.

[27] Boroson DM, Robinson BS, Murphy DV, Burianek DA, Khatri F, Kovalik JM, Sodnik Z, Cornwell DM. Overview and results of the lunar laser communication demonstration. *Free-Space Laser Communication and Atmospheric Propagation XXVI*, *Proc. SPIE*, vol. 8971, Hemmati H, Boroson DM (eds.), 2014; 89 710S.

[28] Oaida BV, Wu W, Erkmen BI, Biswas A, Andrews KS, Kokorowski M, Wilkerson M. Optical link design and validation testing of the optical payload for lasercomm science (OPALS) system. *Free-Space Laser Communication and Atmospheric Propagation XXVI*, *Proc. SPIE*, vol. 8971, Hemmati H, Boroson DM (eds.), 2014; 89 710U.

[29] Giggenbach D. Optimierung der optischen freiraumkommunikation durch die turbulente atmosphäre - focal array receiver. PhD Thesis, Universität der Bundeswehr München 2004.

[30] International Telecommunication Union (ITU). Recommendation ITU-R P.1621-2: Propagation data required for the design of earth-space systems operating between 20 thz and 375 thz jul 2015.

[31] Andrews LC, Philips RL. *Laser Beam Propagation through Random Media*. 2nd edn., SPIE Press: Bellingham, 2005.

[32] Fried DL. Anisoplanatism in adaptive optics. *J. Opt. Soc. Am.* 1982; **72**(1):52–61.

[33] Tyler GA. Bandwidth considerations for tracking through turbulence. *J. Opt. Soc. Am. A* 1994; **11**(1):358–367.

[34] Churnside JH. Aperture averaging of optical scintillations in the turbulent atmosphere. *Appl. Opt.* 1991; **30**(15):1982–1994.

[35] Morello A, Mignone V. DVB-S2: the second generation standard for satellite broad-band services. *Proc. IEEE* 2006; **94**(1):210–227, doi:10.1109/JPROC.2005.861013.

[36] Giggenbach D. Optical free space links for satellite-ground communications. *7th Advanced Satellite Multimedia Systems Conference (ASMS) - Invited Tutorial*, 2014.

[37] Dat PT, Bekkali A, Kazaura K, Wakamori K, Suzuki T, Matsumoto M, Higashino T, Tsukamoto K, Komaki S. Studies on characterizing the transmission of rf signals over a turbulent fso link. *Opt. Express* 2009; **17**(10):7731–7743.

[38] Dimitrov S, Haas H. Information rate of OFDM-based optical wireless communication systems with nonlinear distortion. *J. Lightwave Technol.* 2013; **31**(6):918–929.

[39] Kazaura K, Wakamori K, Matsumoto M, Higashino T, Tsukamoto K, Komaki S. Rofso: a universal platform for convergence of fiber and free-space optical communication networks. *Communications Magazine, IEEE* 2010; **48**(2):130–137.

[40] Sova RM, Sluz JE, Young DW, Juarez JC, Dwivedi A, Demidovich INM, Graves JE, Northcott M, Douglass J, Phillips J, *et al.*. 80 Gb/s free-space optical communication demonstration between an aerostat and a ground station. *Free-Space Laser Communications VI*, *Proc. SPIE*, vol. 6304, Majumdar AK, Davis CC (eds.), 2006; 630 414.

[41] Tsukamoto K, Higashino T, Nakamura T, Takahashi K, Aburakawa Y, Komaki S, Wakamori K, Suzuki T, Kazaura K, Shah AM, *et al.*. Development of radio on free space optics system for ubiquitous wireless. *Progress In Electromagnetics Research Symposium*, vol. 4, PIERS Online, 2008; 96–100.

[42] Wang Z, Zhong W, Fu S, Lin C. Performance comparison of different modulation formats over free-space optical (fso) turbulence links with space diversity reception technique. *Photonics Journal, IEEE* 2009; **1**(6):277–285.

[43] Giggenbach D, Barrios R, Moll F, Mata-Calvo R, Bobrovskyi S, Huber F, Johnson-Amin N, Heine F, Gregory M. EFAL: EDRS feeder link from antarctic latitudes - preliminary results of site investigations, availability, and system requirements. *International Conference on Space Optical Systems and Applications (ICSOS)*, 2014.

[44] Optilab. *Er/Yb Doped Fiber Amplifier +40 dBm*. Optilab, 2015. URL `https://www.optilab.com/eydfa`.

[45] Group S. *ISRUZ Product Line* 1.5 μm *CW High Power Fiber Lasers*. 3SP Group, 2015. URL `http://www.3spgroup.com/data/File/Tech/Manlight/3SP_ISRUZ_Nov2012.pdf`.

[46] "Optical Reliable feeder Link Assessment". Feasibility assessment of optical technologies & techniques for reliable high capacity feeder links. *Technical Report Final Report*, ESA Contract: 21991/08/NL/US 2010.

[47] "Maxim Integrated". *Data Converters*. Online: http://www.maximintegrated.com/en/products/analog/data-converters.html, 2014.

[48] Liva G, Matuz B, Paolini E, Chiani M. Pivoting algorithms for maximum likelihood decoding of LDPC codes over erasure channels. *Proc. of IEEE GLOBECOM 2009*, 2009; 1–6.

[49] Kweon G. Noise figure of optical amplifiers. *J Korean Phys. Soc.* 2002; **41**(5):617–628.

[50] Hudson RD. *Infrared System Engineering*. John Wiley & Sons: New York, 1969.

[51] Arnon S, Kopeika NS, Kedar D, Zilberman A, Arbel D, Livne A, Guelman M, Orenstain M, Ginati HMA. Performance limitation of laser satellite communication due to vibrations and atmospheric turbulence: down-link scenario. *Int. J. Satell. Commun. Network* 2003; **21**:561–573.

[52] Giggenbach D, Henniger H. Fading-loss assessment in atmospheric free-space optical communication links with on-off keying. *Opt. Eng.* 2008; **47**(4):046 001.

[53] Takenaka H, Toyoshima M, Takayama Y. Experimental verification of fiber-coupling efficiency for satellite-to-ground atmospheric laser downlinks. *Opt. Express* 2012; **20**(4):15 301–15 308.

[54] Yu M, Li J, Ricklin J. Efficient forward error correction coding for free-space optical communications. *Free-Space Laser Communications IV*, *Proc. SPIE*, vol. 5550, Ricklin JC (ed.), 2004; 344–353.

[55] Churnside JH, Shaik K. *Atmospheric Propagation Issues Relevant to Optical Communications*. National Oceanic and Atmospheric Administration: Boulder, CO, USA, 1989.

Table 1: Link budget, in the uplink direction, for AT and DT options, for OGS locations Tenerife (2300 m altitude) and Madrid (667 m altitude). The GEO satellite is assumed to be located at 9 °E. Transmitted power always refers to average power. Three signal bandwidths are considered: 36 MHz (Signal A), 225 MHz (Signal B) and 450 MHz (Signal C).

	Tenerife			Madrid		
Parameter	Signal A	Signal B	Signal C	Signal A	Signal B	Signal C
Tx aperture diameter [cm]	24.60	24.60	24.60	10.02	10.02	10.02
Tx divergence [μrad]	5.67	5.67	5.67	13.93	13.93	13.93
Link distance [km]	37506.69	37506.69	37506.69	37879.70	37879.70	37879.70
Elevation angle [°]	46.70	46.70	46.70	41.50	41.50	41.50
Fried parameter [cm]	57.14	57.14	57.14	23.87	23.87	23.87
Angular beam wander [μrad]	2.43	2.43	2.43	5.84	5.84	5.84
Greenwood frequency [Hz]	15.40	15.40	15.40	21.99	21.99	21.99
Scintillation index	0.0103	0.0103	0.0103	0.0546	0.0546	0.0546
Tx antenna gain [dB]	113.06	113.06	113.06	105.26	105.26	105.26
Tx optical loss [dB]	-3.01	-3.01	-3.01	-3.01	-3.01	-3.01
Free-space loss [dB]	-289.66	-289.66	-289.66	-289.75	-289.75	-289.75
Atmospheric attenuation [dB]	-0.14	-0.14	-0.14	-0.33	-0.33	-0.33
Cloud margin [dB]	-3.00	-3.00	-3.00	-3.00	-3.00	-3.00
Strehl ratio loss [dB]	-1.14	-1.14	-1.14	-1.10	-1.10	-1.10
Beam wander loss [dB]	-5.20	-5.20	-5.20	-4.98	-4.98	-4.98
Scintillation margin [dB]	-2.28	-2.28	-2.28	-4.44	-4.44	-4.44
Rx antenna gain [dB]	114.10	114.10	114.10	114.10	114.10	114.10
Rx optical loss [dB]	-3.01	-3.01	-3.01	-3.01	-3.01	-3.01
Fiber coupling loss [dB]	-0.89	-0.89	-0.89	-0.89	-0.89	-0.89
Total loss [dB]	-81.17	-81.17	-81.17	-91.15	-91.15	-91.15
Tx power for AT option [W]	5.00	5.00	5.00	20.00	20.00	20.00
Total Rx power [dBm]	-44.17	-44.17	-44.17	-48.14	-48.14	-48.14
Total Background power [dBm]	-103.54	-103.54	-103.54	-103.84	-103.84	-103.84
SNR (AT option) [dB]	30.63	22.68	19.67	25.0	17.12	14.12
Tx power for DT option [W]	2.50	9.00	15.00	25.00	—	—
SNR for OOK (DT option) [dB]	16.05	16.05	16.00	16.07	—	—
BER (DT option)	1.10E-10	1.10E-10	2.14E-10	9.72E-11	—	—
Tx power for DT+FEC option [W]	1.20	3.80	6.50	12.00	38.00	—
SNR for OOK (DT+FEC option) [dB]	10.91	10.85	11.12	10.93	10.87	—
BER (DT+FEC option)	1.52E-10	2.90E-10	1.64E-10	1.08E-10	2.15E-10	—